Analyst

ROYAL SOCIETY OF CHEMISTRY

COMMUNICATION

View Article Online
View Journal | View Issue

Cite this: *Analyst*, 2021, **146**, 816

Received 19th November 2020,
Accepted 10th December 2020

DOI: 10.1039/d0an02250k

rsc.li/analyst

Photo-driven self-powered biosensors for ultrasensitive microRNA detection based on metal–organic framework-controlled release behavior†

Ying Yu,[a] Xiuli Xu, *[b] Qiao Su,[c,d] Tengfei Fu,[c,d] Wenquan Liu[c,d] and Guangquan Chen[c,d]

We developed a "signal-on" self-powered biosensing strategy by taking full advantage of both photoelectrochemical biofuel cells (PBFCs) and metal–organic framework (MOF)-controlled release behavior for ultrasensitive microRNA assay. PBFC-based self-powered sensors have the unique characteristics of non-requirement of external power sources, simple fabrication process, miniature size, good anti-interference ability and low cost. Furthermore, based on the target microRNA-induced release of the electron donor ascorbic acid and the high catalytic ability of the biocathode to catalyse the oxygen reduction reaction, photo-driven self-powered biosensors for ultrasensitive microRNA detection were successfully realized. The as-proposed signal-on biosensor not only provides a simple and effective strategy, but also possesses the merits of a wide dynamic concentration response range and high sensitivity for microRNA detection, with a limit of detection down to 0.16 fM.

MicroRNAs (miRNAs) are small non-coding RNAs (18 nt to 24 nt), which are relevant to various biological and pathological processes.[1,2] Their dysregulated expression is often involved in multiple types of cancer, so they have been widely applied as important biomarkers for cancer diagnosis and treatment.[3,4] To date, great efforts have been made for miRNA detection, such as electrochemistry,[5–7] fluorescence,[8,9] electrochemiluminescence,[10,11] surface-enhanced Raman scattering,[12,13] quantitative reverse transcription polymerase chain reaction,[14,15] and so forth. Although the above-mentioned strategies could improve the flexibility and sensitivity of miRNA assays, the complicated configuration and requirement of skilled operators limited their practical applications. Thus, it is indispensable to explore a simple and easy-to-operate strategy for miRNA detection.

Self-powered biosensors have been extensively applied in immunoassay,[16] cytosensing,[17] environmental monitoring,[18] disease diagnosis[19–22] and food safety,[23,24] because of their inherent merits such as simple fabrication process, non-requirement of external power sources, and low cost.[25–27] However, the evolution of self-powered biosensors still suffered from the limitations of bioenzymes, including the controversy over the catalytic mechanism of anodic enzymes (for example, glucose oxidase) and difficulties in long-term storage. To solve the above issues, photoelectrochemical biofuel cell (PBFC)-based self-powered biosensors have emerged due to their direct photo-oxidation characteristic and non-requirement of anodic enzymes or noble metals as anodes.[28,29] Nevertheless, to improve the anti-interference ability and reduce false-positive readout,[30,31] the "signal-on" strategy based on metal–organic framework (MOF)-controlled release behavior was cleverly combined with PBFC-based self-powered biosensors. In consequence, the "signal-on" PBFC-based self-powered biosensors would be an ideal protocol to accurately detect miRNAs with excellent anti-interference ability.

Herein, "signal-on" PBFC-based self-powered biosensors based on MOF-controlled release behavior were constructed for ultrasensitive miRNA detection, which were composed of a carbon nitride/gold nanoparticles (g-C_3N_4/AuNPs) photoanode and a graphene oxide/carbon nanotubes/AuNPs/bilirubin oxidase (GO/CNTs/AuNPs/BOD) biocathode. In this work, the MOF-controlled release strategy is crucial for the use of self-powered biosensors to accurately detect miRNA (miRNA-21 as the model). The complementary strand of miRNA-21 (csDNA), as the biogate, would cap the PDDA-modified MOF (PMOF) through electrostatic adsorption, which encapsulated ascorbic

[a]*Coastal Science and Marine Policy Center, First Institute of Oceanography, Ministry of Natural Resources, Qingdao, 266061, P.R China*
[b]*School of Ocean Sciences, China University of Geosciences, Beijing, 100083, P. R. China. E-mail: xuxl@cugb.edu.cn; Tel: +86-10-82319124*
[c]*Key Laboratory of Marine Sedimentology and Environmental Geology, First Institute of Oceanography, Ministry of Natural Resources, Qingdao 266061, P.R China*
[d]*Laboratory for Marine Geology, Qingdao National Laboratory for Marine Science and Technology, Qingdao 266061, P.R China*

†Electronic supplementary information (ESI) available: Experimental section. TEM image of g-C_3N_4/AuNPs; optimization of experimental conditions; CVs of different biocathodes with N_2 or O_2; sequences of the oligonucleotides used in the experiments; comparison of the analytical performance for miRNA assay by our method and those reported in the literature. See DOI: 10.1039/d0an02250k

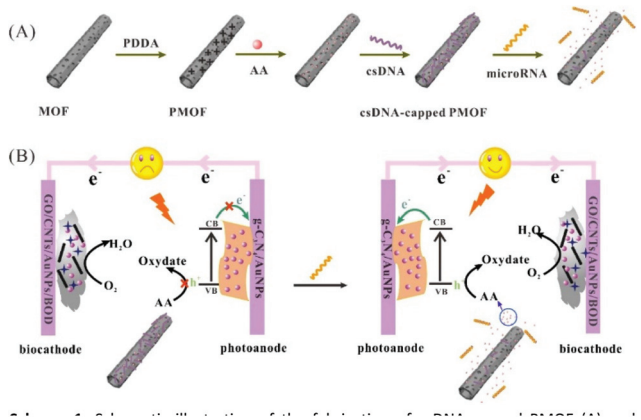

Scheme 1 Schematic illustration of the fabrication of the csDNA-capped PMOF (A) and PBFC-based self-powered biosensors for miRNA detection (B).

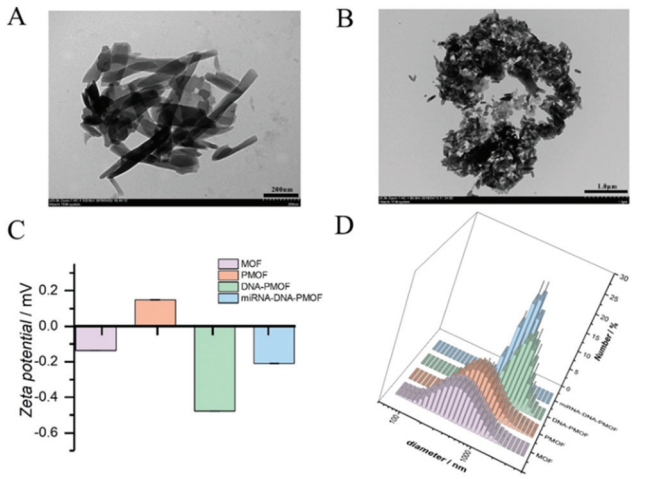

Fig. 1 TEM images of the MOF (A) and the PMOF (B); zeta potential (C) and dynamic light scattering (D) of the MOF, PMOF, DNA–PMOF and miRNA–DNA–PMOF.

acid (AA) that entered the pores *via* diffusion into the PMOF (Scheme 1A). The self-powered biosensors were constructed based on the above csDNA-capped PMOF; the principle is shown in Scheme 1B. In the absence of the target miRNA-21, AA was encapsulated in the pores of the PMOF and a low open circuit voltage (E^{OCV}) was observed. Once the target miRNA-21 was introduced, it could hybridize with the capped csDNA to form the rigid DNA–RNA hetero-duplex structure, which would detach from the PMOF surface, and then the biogate on the csDNA-capped PMOF was efficiently opened, resulting in the controlled release of the entrapped AA. Meanwhile, the AA released was directly oxidized on the photoanode by photo-generated holes to generate electrons, and the electrons were transported to the biocathode through an external circuit to achieve oxygen reduction, thus producing a high E^{OCV}. Overall, the proposed "signal-on" self-powered biosensors were successfully realized for the accurate detection of miRNA-21 based on the MOF-controlled release strategy. This strategy perfectly combined the self-powered biosensor and the controlled release system, and provided a new idea for constructing a "signal-on" biosensor to accurately detect miRNA.

As the key to launch the biosensors, the MOF and its derivatives were characterized by transmission electron microscopy (TEM), zeta potential analysis and dynamic light scattering. As shown in Fig. 1B, the morphology of the PMOF showed almost no change compared with that of the MOF (Fig. 1A). Besides, the zeta potential analysis was carried out to confirm the successful construction of the layer-by-layer assembly of miRNA–DNA–PMOF (Fig. 1C). After PDDA was modified, the zeta potential value of the PMOF changed from −0.13 to +0.16 mV, suggesting the adsorption of positively charged PDDA. With the introduction of the negatively charged DNA, the zeta potential value greatly reduced to −0.5 mV, demonstrating that DNA was adsorbed on the PMOF surface through electrostatic adsorption. The zeta potential value could recover to some extent because the DNA–RNA hetero-duplex was detached from the PMOF. In addition, dynamic light scattering was also implemented to verify the protocol. As shown in Fig. 1D, the particle size gradually increased after the modification of PDDA and DNA, implying successful fabrication. However, once the target miRNA existed, the particle size of miRNA–DNA–PMOF would be reduced to a certain extent compared with that of DNA–PMOF, indicating the detachment of the DNA–RNA hetero-duplex. All of the above results affirmed the successful construction of the csDNA-capped PMOF and the ability for target-induced csDNA liberation.

For the photoanode, g-C_3N_4/AuNPs were selected as the substrate materials owing to their excellent photoelectric capability. Fig. S1† shows that AuNPs were uniformly decorated on the surface of the g-C_3N_4 nanosheets, indicating the successful synthesis of g-C_3N_4/AuNPs. Furthermore, we investigated the differential pulse voltammetric (DPV) and photocurrent responses with different concentrations of the target miRNA-21 to verify the feasibility of the biosensing strategy. As illustrated in Fig. 2A, the current value increased with the increase of the miRNA-21 concentration, which could be attributed to the fact that miRNA with a higher concentration would

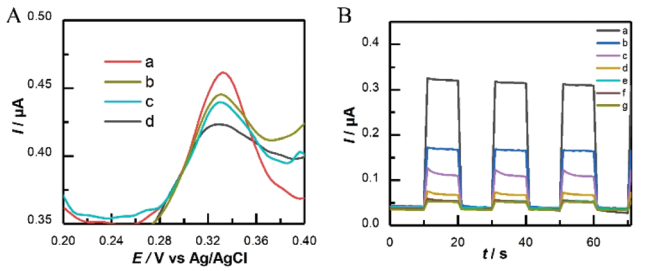

Fig. 2 (A) DPV responses of AA at the bare ITO electrode in the presence of miRNA-21 with different concentrations (from d to a: 1, 10, 100, and 1000 fM); (B) photocurrent responses of g-C_3N_4/AuNPs in the presence of miRNA-21 with different concentrations (from g to a: 0.1, 0.5, 1, 5, 10, 100, and 1000 fM).

open more biogates; thus more AA were released. Similarly, the photocurrent responses also proved the release process controlled by the target miRNA (Fig. 2B). The photocurrent intensity was positively correlated with the miRNA concentration since the more released AA induced by miRNA could consume more holes to avoid electron–hole recombination, thereby generating higher photocurrent. The above-mentioned results confirmed the release process of the entrapped AA, which further suggested the feasibility for assembling the self-powered biosensor. Apart from this, to realize the optimal performance of PBFC-based self-powered biosensors for miRNA detection, the concentration of AA as well as csDNA, the block time of csDNA, and the release time of AA were optimized (Fig. S2†).

Under the circumstances, the biocathode as the electron acceptor also had a vital influence on the performance of the self-powered biosensor. Herein, electrochemical impedance spectroscopy (EIS) was employed to monitor the assembling process of the biocathode. As shown in Fig. 3A, the charge-transfer resistance (R_{ct}) value of the ITO/GO/CNTs/AuNPs electrode (140 Ω, curve a) was smaller than that of the bare ITO electrode (300 Ω, curve c), demonstrating the excellent conductivity of GO/CNTs/AuNPs composites. Besides, after the modification of PBSE, the R_{ct} value of the ITO/GO/CNTs/AuNPs/PBSE electrode (380 Ω, curve b) showed a slight increase. And when BOD was immobilized onto the electrode surface, the R_{ct} value sharply increased (655 Ω, curve d), attributed to the fact that the non-electroactive BOD prevented the redox probes from reaching the electrode surface. Nevertheless, cyclic voltammetry (CV) was carried out to explore the bioelectrocatalytic behavior of the biocathode in Fig. 3B. The cathodic current increased by 100 μA at −0.2 V in the O_2-saturated solution compared with that under the N_2 system, illustrating the efficient catalytic ability of the biocathode. As a control, the biocathode without BOD had almost no ability to catalyze oxygen reduction (Fig. S3†), further indicating the catalytic ability of BOD. All of the above results demonstrated that the as-prepared biocathode exhibited excellent conductivity and outstanding catalytic ability, which laid a solid foundation for the fabrication of PBFC-based self-powered biosensors.

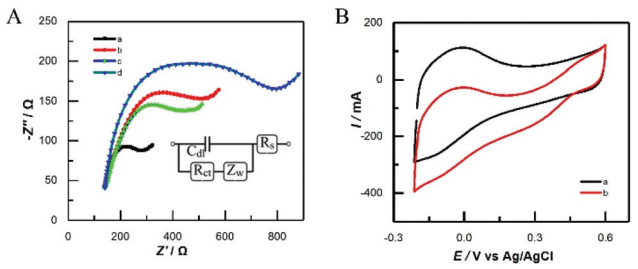

Fig. 3 (A) EIS curves of different modified ITO electrodes: (a) ITO/GO/CNTs/AuNPs, (b) ITO/GO/CNTs/AuNPs/PBSE, (c) bare ITO electrode, and (d) ITO/GO/CNTs/AuNPs/PBSE/BOD. (B) CVs of the ITO/GO/CNTs/AuNPs/PBSE/BOD biocathode in PB (pH = 7.4) saturated with N_2 (a) or O_2 (b). Scan rate = 50 mV s^{-1}.

By integrating the photoanode and biocathode, the PBFC-based self-powered biosensor was constructed for ultrasensitive miRNA detection. As illustrated in Fig. 4A, in the absence of the target miRNA, the E^{OCV} value of the self-powered biosensor was only 0.12 V. However, when the target miRNA induced the release of AA through forming the rigid DNA–RNA hetero-duplex structure, the E^{OCV} value of the self-powered biosensor gradually increased with the increase of the miRNA concentration (curve from g to a). Furthermore, Fig. 4B shows a good linear relationship between the E^{OCV} value and the miRNA concentration over a linear range of 0.5 to 1000 fM. The linear equation was $E^{OCV} = 0.160 + 0.037c$ (coefficient of determination $R^2 = 0.998$), and the detection limit of the self-powered biosensor was 0.16 fM (S/N = 3), which was commensurate with or superior to those of the reported methods (Table S2†). Although the detection limit of the as-prepared self-powered biosensor was not the lowest, the ingenious amalgamation of the MOF-controlled release strategy and the PBFC-based self-powered biosensor provided more possibilities for biomedical detection and treatment.

To confirm the selectivity of the as-proposed self-powered biosensor, a series of analogous miRNAs, such as miRNA-143, miRNA-141, miRNA-155, and miRNA-199a, were selected as the interferences. As shown in Fig. 4C, in comparison with the interferences, only miRNA-21 could generate a relatively high E^{OCV} value, ascribing to the high specificity of the base pairing reaction. The above result demonstrated that the as-prepared self-powered biosensor had excellent selectivity for miRNA detection.

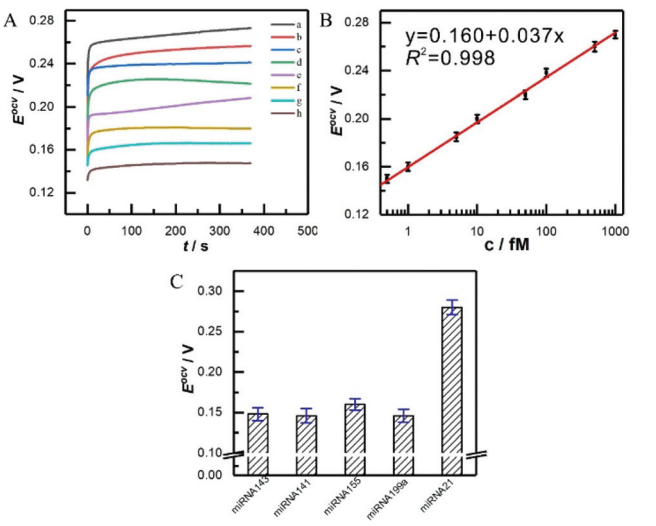

Fig. 4 (A) E^{OCV} of the proposed biosensor in the presence of miRNA-21 with different concentrations (from h to a: 0.5, 1, 5, 10, 50, 100, 500, and 1000 fM). (B) The plot of E^{OCV} *vs.* the logarithm of the miRNA-21 concentration. (C) Selectivity analysis for miRNA-21 by monitoring E^{OCV} with 1 pM of interferences and miRNA-21. Error bars represent the standard deviation of an average value from independent measurements of three biosensors.

Conclusions

In summary, we proposed "signal-on" PBFC-based self-powered biosensors based on MOF-controlled release behavior for ultrasensitive miRNA detection. Encouragingly, the as-proposed self-powered biosensor possessed a wide dynamic concentration response range and high sensitivity for miRNA detection, which could be attributed to the ingenious design of the MOF-controlled release strategy to enable the "signal-on" detection of miRNA. In this work, the ingenious combination of the PBFC-based self-powered biosensor and the MOF-controlled release strategy not only improved the anti-interference ability of the biosensor, but also provided a fresh idea for ultrasensitive miRNA detection.

Conflicts of interest

There are no conflicts of interest to declare.

Acknowledgements

This research was financially supported by the National Natural Science Foundation of China (U1806212) and the Basic Scientific Fund for National Public Research Institutes of China (2019Q01).

Notes and references

1 R. Deng, K. Zhang and J. Li, *Acc. Chem. Res.*, 2017, **50**, 1059–1068.
2 D. P. Bartel, *Cell*, 2004, **116**, 281–297.
3 G. A. Calin and C. M. Croce, *Nat. Rev. Cancer*, 2006, **6**, 857–866.
4 H. Dong, J. Lei, L. Ding, Y. Wen, H. Ju and X. Zhang, *Chem. Rev.*, 2013, **113**, 6207–6233.
5 Y. Y. Bai, Z. Wu, C. M. Xu, L. Zhang, J. Feng, D. W. Pang and Z. L. Zhang, *Anal. Chem.*, 2020, **92**, 853–858.
6 P. Gai, C. Gu, H. Li, X. Sun and F. Li, *Anal. Chem.*, 2017, **89**, 12293–12298.
7 T. Hou, N. Xu, W. Wang, L. Ge and F. Li, *Anal. Chem.*, 2018, **90**, 9591–9597.
8 J. Li, S. Cai, B. Zhou, X. Meng, Q. Guo, X. Yang, J. Huang and K. Wang, *Chem. Commun.*, 2020, **56**, 6126–6129.
9 X. Zhao, L. Zhang, W. Gao, X. Yu, W. Gu, W. Fu and Y. Luo, *ACS Appl. Mater. Interfaces*, 2020, **12**, 35958–35966.
10 T. B. Gao, J. J. Zhang, J. Wen, X. X. Yang, H. B. Ma, D. K. Cao and D. Jiang, *Anal. Chem.*, 2020, **92**, 1268–1275.
11 L. Lu, C. Liu, T. Kang, X. Wang, G. Guo and W. Miao, *Sens. Actuators, B*, 2018, **255**, 35–41.
12 S. Ye, X. Li, M. Wang and B. Tang, *Anal. Chem.*, 2017, **89**, 5124–5130.
13 Y. He, X. Yang, R. Yuan and Y. Chai, *Anal. Chem.*, 2017, **89**, 2866–2872.
14 C. C. Pritchard, H. H. Cheng and M. Tewari, *Nat. Rev. Genet.*, 2012, **13**, 358–369.
15 Z. Hu, F. Xu, G. Sun, S. Zhang and X. Zhang, *Chem. Commun.*, 2020, **56**, 5409–5412.
16 Y. Wang, L. Ge, P. Wang, M. Yan, J. Yu and S. Ge, *Chem. Commun.*, 2014, **50**, 1947–1949.
17 X. Pang, C. Cui, M. Su, Y. Wang, Q. Wei and W. Tan, *Nano Energy*, 2018, **46**, 101–109.
18 X. Li, D. Li, Y. Zhang, P. Lv, Q. Feng and Q. Wei, *Nano Energy*, 2020, **68**, 104308.
19 C. Gu, P. Gai, X. Kong, T. Hou and F. Li, *Anal. Chem.*, 2020, **92**, 5426–5430.
20 C. Gu, X. Kong, X. Liu, P. Gai and F. Li, *Anal. Chem.*, 2019, **91**, 8697–8704.
21 L. Wang, H. Shao, X. Lu, W. Wang, J. R. Zhang, R. B. Song and J. J. Zhu, *Chem. Sci.*, 2018, **9**, 8482–8491.
22 L. Wang, H. Shao, W. Wang, J. Zhang and J. Zhu, *Nano Energy*, 2018, **44**, 95–102.
23 P. Gai, C. Gu, T. Hou and F. Li, *Anal. Chem.*, 2017, **89**, 2163–2169.
24 C. Gu, P. Gai, T. Hou, H. Li, C. Xue and F. Li, *ACS Appl. Mater. Interfaces*, 2017, **9**, 35721–35728.
25 Y. Chen, W. Ji, K. Yan, J. Gao and J. Zhang, *Nano Energy*, 2019, **61**, 173–193.
26 M. Grattieri and S. D. Minteer, *ACS Sens.*, 2017, **3**, 44–53.
27 M. Zhou, N. Zhou, F. Kuralay, J. R. Windmiller, S. Parkhomovsky, G. Valds-Ramrez, E. Katz and J. Wang, *Angew. Chem.*, 2012, **124**, 2740–2743.
28 K. Yan, Y. Yang, O. K. Okoth, L. Cheng and J. Zhang, *Anal. Chem.*, 2016, **88**, 6140–6144.
29 P. Gai, X. Kong, S. Zhang, P. Song and F. Li, *Chem. Commun.*, 2020, **56**, 7116–7119.
30 Y. Chen, J. Gao, K. Yan, X. Yao, Y. Liu and J. Zhang, *Sens. Actuators, B*, 2020, **316**, 128130.
31 X. Du, D. Jiang, Q. Liu, N. Hao and K. Wang, *Anal. Chem.*, 2019, **91**, 1728–1732.